Space-charge-limited, two-dimensional unmagnetized flow in a wedge geometry

A. Rokhlenko[a] and J. L. Lebowitz[b]
Department of Mathematics, Rutgers University, Piscataway, New Jersey 08854-8019, USA

(Received 17 August 2007; accepted 20 October 2007; published online 20 December 2007)

This paper studies the space-charge-limited current in an infinite wedge geometry in two dimensions. This geometry permits a reduction of the problem to a set of easily solved ordinary differential equations. The system, though very simplified, exhibits features similar to those expected to occur in many realistic systems with inhomogeneous electric fields. We obtain, in particular, a universal form for the particle trajectories and a nonmonotone charge distribution with accumulation at both the cathode and the anode. The explicit solution of the model can be useful for testing numerical schemes. The case of a very low density current is also considered. Relaxation of the geometrical limitations of the model are studied using conformal mapping techniques. Possible applications to realistic systems, which can be tested by simple experiments, are presented. © *2007 American Institute of Physics*. [DOI: 10.1063/1.2822471]

I. INTRODUCTION

The generalization of the one-dimensional Child–Langmuir results for the space-charge-limited current to two and three dimensions is a difficult task. It can be simplified, somewhat, by imposing a very strong magnetic field in the flow direction.[1–3] This produces a sharp boundary for the space-charge region and causes a strong increase (even divergence in the limit when the magnetic field is infinite) of the current density at the boundary, the so-called current wings.[1,2] On the other hand, both experiments and computations[3] show that the change in the total current due to the high density of the wing current is small, except for narrow beams. When the magnetic field is weak or absent the stream lines of the current are not straight and the description of the flow must include the dynamical equations for the motion of charged particles in two or three dimensions. We consider here a simple geometry for the space-charge-limited flow without magnetic field where the hydrodynamic equations can be effectively solved for the case of infinite cathode emissivity. The result is a complete picture of the field, current, and charge density distribution along with the trajectories of the individual particles.

We also consider corrections to this solution for more realistic geometries. This suggests (i) a test case for algorithms used in numerical calculations in more complicated systems and (ii) some experiments whose results can be compared with our theory.

II. SYSTEM GEOMETRY AND GENERAL SETUP

We consider a wedge geometry with the positive half plane $x>0$, $y=0$ as the cathode, whose potential is zero, while the half plane, which makes an angle Θ with the cathode, is the anode at potential V; see the cross section of this system in the plane $z=0$ in Fig. 1.

In the absence of the space charge the potential φ at a point (r,θ) depends only on θ, $\varphi=V\theta/\Theta$, $0\leq\theta\leq\Theta$. In Fig. 1 the radii are a set of equidistant equipotentials while the circular arcs represent the electric field lines. The solid curved line is a particle trajectory in the vacuum field (see below). When the cathode has infinite emissivity there will be a nonzero charge and current density, as in Refs. 1–3, and one has to solve a set of equations which determine the stationary state of the system. These will involve the potential $\varphi(r,\theta)$, the velocity field of the charges $\mathbf{u}(r,\theta)$, and the space charge density $en(r,\theta)$. They consist of the Poisson equation, the plasma hydrodynamic equation,[4] and the current continuity relation,

$$\Delta\varphi = 4\pi en(r,\theta), \tag{1}$$

$$(\mathbf{u}\nabla)\mathbf{u} = \frac{e}{m}\nabla\varphi, \tag{2}$$

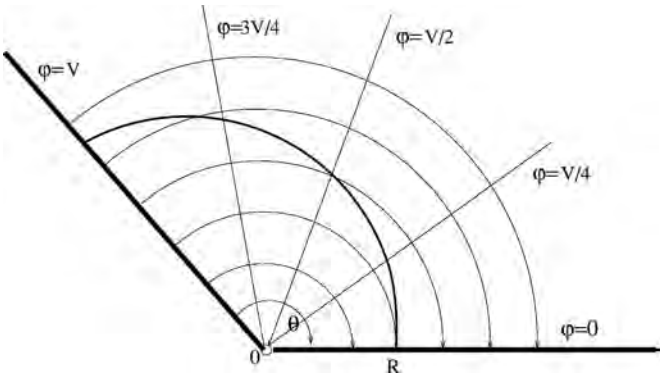

FIG. 1. Cross section of the system with vacuum electric field. The thick curve shows a single charge trajectory.

[a]Electronic mail: rokhlenk@math.rutgers.edu.
[b]Also with the Department of Physics, Rutgers University, Piscataway, New Jersey 08854-8019, USA.

$$\nabla(n\mathbf{u}) = 0. \tag{3}$$

Here e and m are the charge and mass of the particles carrying the current. Equations (1)–(3) are to be solved subject to the boundary conditions

$$\varphi(r,0) = 0, \quad \varphi(r,\Theta) = V, \tag{4}$$

and

$$\frac{\partial\varphi}{\partial\theta}(r,0) = 0, \tag{5}$$

where Eq. (5) expresses the fact[2] that the flow of electrons from the cathode is limited by the space charge only.

We assume the flow to be potential, i.e., $[\nabla\times\mathbf{u}]=0$, as it is done usually in such calculations. Then, in the case where the charges are emitted with zero speed $u(r,0)=0$, Eq. (2) can be reduced to the energy conservation relation $mu^2(r,\theta)/2=e\varphi(r,\theta)$, and one more equation which involves the unit vector $\mathbf{I}=\mathbf{u}/u$,

$$(\mathbf{I}\nabla)\phi = [\mathbf{I}\times\nabla]_\perp \ln u = -\sin\phi\,\frac{\partial \ln u}{\partial x} + \cos\phi\,\frac{\partial \ln u}{\partial y}. \tag{6}$$

In Eq. (6) we have set $\mathbf{I}=\{\cos\phi, \sin\phi\}$ in the Cartesian (x,y) plane and projected the vector product into this plane. There are three scalar unknown functions in the set of Eqs. (1)–(3): $\varphi(r,\theta)$, $n(r,\theta)$, and $\phi(r,\theta)$, where the angle ϕ between $\mathbf{u}(r,\theta)$ and the x-axis determines the current direction. Along with ϕ we will use the angle between the particle velocity and the direction along the circular arc at the same point (see Fig. 1) $\beta(\theta)=\frac{\pi}{2}+\theta-\phi$. The boundary conditions for ϕ and β are

$$\phi(r,0) = \frac{\pi}{2}, \quad \beta(0) = 0. \tag{7}$$

We show below a surprisingly simple solution in this setting whose spatial structure allows some generalizations without too much effort. Note that in the case of unlimited cathode emission, but with $u(r,0)\neq 0$, our method works with small modifications. If the intensity of the cathode emission is determined by the electric field and/or is limited by some other conditions, but the initial speed $u(r,0)=0$, only Eq. (5) must be modified. When $u(r,0)$ is a function of x, both Eq. (7) and the energy equation change. Unfortunately we do not see a simple way of solving the problem in such cases.

III. SOLUTION

We now look for a solution for φ as a function of θ alone. In this case Eq. (1) yields

$$n(r,\theta) = \frac{\nu(\theta)}{r^2}, \tag{8}$$

and thus the density of the charged particles is determined by a yet unknown function ν of a single angular variable. Straightforward manipulations now allow to reduction of Eqs. (1)–(3) to three ordinary differential equations in θ

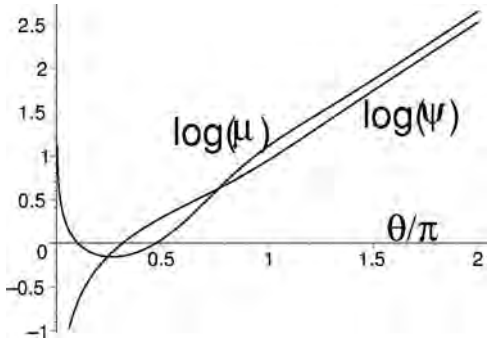

FIG. 2. Space charge density and potential as functions of θ.

$$\frac{d^2\varphi}{d\theta^2} = 4\pi e\nu(\theta), \quad \frac{d\beta}{d\theta} = 1 - \frac{\tan\beta}{2}\frac{d\ln\varphi}{d\theta} = \cos 2\beta + \frac{\sin 2\beta}{2}\frac{d\ln\nu}{d\theta}, \quad \text{for } 0<\theta<\Theta. \tag{9}$$

The full set of boundary conditions consists of Eqs. (4), (5), and (7).

By temporarily neglecting the boundary condition $\varphi(\Theta)=V$ in Eq. (4), we can multiply both functions $\varphi(\theta)$ and $\nu(\theta)$ in Eq. (9) by the some constant C without affecting the solution for $\beta(\theta)$. This allows us to introduce instead of φ and ν the dimensionless functions $\psi=C\varphi$ and $\mu=4\pi eC\nu$, which are governed by the set of four first-order equations

$$\frac{d\beta}{d\theta} = 1 - \frac{f(\theta)\tan\beta}{2\psi}, \quad \frac{d\mu}{d\theta} = \mu\left(2\tan\beta - \frac{f}{2\psi\cos^2\beta}\right),$$

$$\frac{df}{d\theta} = \mu, \quad \frac{d\psi}{d\theta} = f, \tag{10}$$

which come directly from Eq. (9). One more function f is added temporarily in Eq. (10) for convenience. In view of the boundary conditions, Eqs. (4)–(6), we will look for solutions of Eq. (10) with a power law behavior near $\theta=0$, i.e., $\psi\sim\theta^\gamma$, $(\gamma>0)$, and therefore $\beta\sim$const θ. Substituting into Eq. (10) we find $\gamma=4/3$, and thus Eq. (10) is consistent for small θ with the initial conditions

$$\psi \approx \theta^{4/3}, \quad \mu \approx 4\theta^{-2/3}/9, \quad \beta \approx 3\theta/5. \tag{11}$$

After solving Eq. (10), ψ and μ must be multiplied by such a factor $1/C$, whose value makes $\varphi(\Theta)=V$, converts μ into ν, and thus completes the solution. Clearly $C=\psi(\Theta)/V$.

We apply a standard Maple routine for solving Eqs. (10) and (11) as an initial value problem and calculate β,ψ,μ as functions of θ. Reaching the anode terminal point and evaluating $\psi(\Theta)$ we get the solution for φ,ν in the form

$$\varphi(\theta) = \frac{V\psi(\theta)}{\psi(\Theta)}, \quad \nu(\theta) = \frac{V\mu(\theta)}{4\pi e\psi(\Theta)}. \tag{12}$$

The angular dependence of the charge density $\mu(\theta)$ and the potential function $\psi(\theta)$ are shown in Fig. 2 in the logarithmic scale. The space-charge density is divergent near the cathode then decreases until θ reaches $\sim\pi/4$, and for larger θ (which means $\Theta>\pi/4$) it grows as one moves toward the anode.

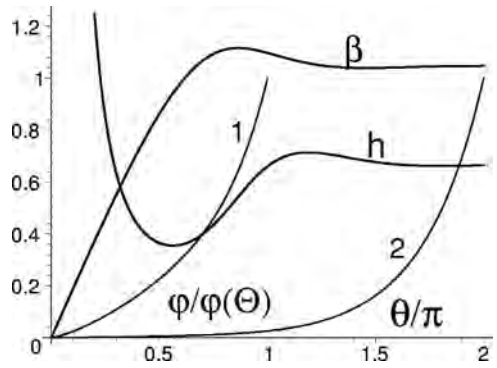

FIG. 3. Direction of flow $\beta(\theta)$ and current parameter $h(\theta)$. Curves 1 and 2 show normalized potentials $\varphi(\theta)/\varphi(\Theta)$ for $\Theta=\pi$ and $\Theta=2\pi$, respectively.

In Fig. 3 we plot the angle $\beta(\theta)$, the normalized potential $\varphi/V=\psi(\theta)/\psi(\Theta)$, and the current parameter $h(\theta)$ [see Eqs. (13) and (14)]; (these functions are independent of r). One can see, especially when $\Theta=2\pi$, that the potential and thus the flow speed sharply increase near the anode. The majority of charged particles, which are plentiful near the origin, can reach the anode without traveling far radially because there is a significant velocity component parallel to the anode (see Fig. 4).

Note that $\psi(\theta)$, which behaves as $\theta^{4/3}$ for small θ, as shown in Eq. (11), grows roughly exponentially (see Fig. 2) when $\theta>1$, in particular, $\psi(\pi)\approx 8.73$, $\psi(2\pi)\approx 337$. Using Eqs. (8) and (12) we evaluate the current density into the anode (i.e., the component normal to it),

$$J(r,\Theta)=en(r,\Theta)u(\Theta)\cos[\beta(\Theta)]=\frac{V^{3/2}}{4\pi r^2}\sqrt{\frac{2e}{m}}h(\Theta). \tag{13}$$

The parameter

$$h(\theta)=\frac{\mu(\theta)\cos[\beta(\theta)]}{\psi(\theta)}, \tag{14}$$

whose graph is given in Fig. 3, becomes almost constant (~ 0.65) for $\theta>\pi$, but it changes very sharply for smaller angles. The oblique incidence of the flow is given by the factor $\cos\beta$ in Eq. (14).

The current density in Eq. (13) has a strong resemblance to the Child–Langmuir constant current density,[5]

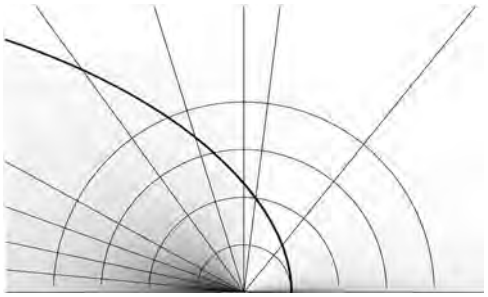

FIG. 4. Structure of the electric field and density of charged particles for $\Theta=\pi$. Half circles show the field stream lines, while the set of radii presents the equidistant equipotentials. The bold curve is a typical particle trajectory.

$$j_0=\sqrt{\frac{2e}{m}}\frac{V^{3/2}}{9\pi d^2}, \tag{15}$$

where d is the distance between two parallel electrodes. The absolute value of the current at an arbitrary point $\theta<\Theta$ has the form

$$j(r,\theta)=\frac{V^{3/2}\mu(\theta)}{4\pi r^2\psi^{3/2}(\Theta)}\sqrt{\frac{2e\psi(\theta)}{m}}, \tag{16}$$

and the angle between the current direction and the x-axis is $\phi=\pi/2+\theta-\beta(\theta)$. We show in Fig. 4 some additional results of the calculation. While the equipotential lines are uniformly distributed when the charge density is negligible (Fig. 1), here they get denser near the anode. This is similar to the Child–Langmuir setup in one dimension. Each radial line in Fig. 4 is an equipotential; starting from the cathode their voltages differ by $V/10$. The background shading density in Fig. 4 exhibits approximately the distribution of the charged particles between the electrodes. The figure is constructed for the case $\Theta=\pi$, but clearly the anode can be placed at any radius without disturbing the field and density inside the angle.

IV. PARTICLE TRAJECTORIES

To understand the structure of the current we calculate now the trajectories of individual particles in their collective field. Writing the equation for a single particle of mass m and charge $-e$, $m\ddot{\mathbf{r}}=e\nabla\varphi$, in polar coordinates we get

$$r^2\ddot{\theta}+2r\dot{r}\dot{\theta}=\frac{e}{m}\frac{\partial\varphi}{\partial\theta},\quad \ddot{r}-r\dot{\theta}^2=\frac{e}{m}\frac{\partial\varphi}{\partial r}, \tag{17}$$

where, as usual, dots denote time derivatives. These two equations are to be solved subject to the initial conditions

$$r(0)=R,\quad \theta(0)=0,\quad \dot{r}(0)=\dot{\theta}(0)=0. \tag{18}$$

The parameter R here gives the initial location of the electron at the cathode, while Eq. (12) determines $\varphi(\theta)$. In dimensionless variables

$$\rho(\tau)=r(t)/R,\quad \tau=\frac{t}{R}\sqrt{\frac{2eV}{m\psi(\Theta)}}, \tag{19}$$

and the particle dynamics is described by the following initial value problem:

$$\frac{d^2\rho}{d\tau^2}=\rho\left(\frac{d\theta}{d\tau}\right)^2,\quad \rho\frac{d^2\rho}{d\tau^2}+\left(\frac{d\rho}{d\tau}\right)^2=\psi(\theta);$$

$$\rho(0)=1,\quad \theta(0)=\frac{d\rho}{d\tau}(0)=\frac{d\theta}{d\tau}(0)=0. \tag{20}$$

Equation (20) determines a universal trajectory $\rho=\rho(\theta)$: the initial point gives the scaling factor R, while the anode potential V and the terminal angle Θ define the time scaling. A simple analysis of Eq. (20), using Eq. (11) near $\theta=0$, yields

$$\theta(t)\approx t^3/8,\quad \rho\approx 1+3t^6/640,\quad \text{when } t\to 0.$$

The solution of the ordinary set of equations, Eq. (20), is straightforward and the calculated trajectory is shown in Fig.

TABLE I. Trajectory $\rho(\theta)$ of an individual particle when emission is unlimited.

θ	0	0.1π	0.3π	0.5π	0.6π	0.7π	0.8π	0.9π	π	1.2π	1.5π	1.8π	1.9π	2π
ρ	1	1.03	1.32	2.29	3.48	5.84	10.7	20.4	38.2	122	619	3117	5369	9257

4 for $\theta<2.28$. The evolution of $\rho(\theta)$ up to $\theta=\pi$ can be seen in Table I.

The distance from the origin as a function of θ grows very fast because the space charge pushes the individual particles away from the place of their concentration near the origin [see Eq. (8)]. Note that $\rho(2\pi)$ is close to 10^4: after turning a complete circle the particles almost run away.

The consistency of our calculations in Secs. III and IV can be checked by comparing the current I_r through a ray $r \geq r_1$, placed at the angle θ, with the cathode current I_c,

$$I_r(r_1,\theta)=\int_{r_1}^{\infty} J(r,\theta)dr=\frac{h(\theta)}{4\pi r_1}\sqrt{\frac{2e}{m}}\left[\frac{V\psi(\theta)}{\psi(\Theta)}\right]^{3/2},$$

$$I_c(r_2,0)=\int_{r_2}^{\infty} j(r,0)dr=\frac{\sqrt{2e/m}}{9\pi r_2}\left[\frac{V}{\psi(\Theta)}\right]^{3/2}.$$

It is clear that these two currents must be equal when $r_1=r_2\rho(\theta)$ because of the universal properties of all trajectories. Therefore using Eq. (19) we have without solving Eq. (17),

$$\rho(\theta)=9h(\theta)\psi^{3/2}(\theta)/4. \tag{21}$$

Equation (21) agrees with the solution of Eq. (20) and Table I in particular.

V. EXTENSION TO MORE REALISTIC GEOMETRIES

The stationary solution for the flow in Secs. II–IV is obtained for a very idealized setup when the electrodes are infinite and there is no interelectrode gap. The singular field at the vertex creates the divergent charge density [Eq. (8)] and there is an infinite total charge accumulation in a sector $0<r\leq k$, $0<\theta\leq\Theta$,

$$eN(k)=e\int_0^k rdr\int_0^{\Theta} n(r,\theta)d\theta=\infty.$$

Despite this the electric field is finite away from the origin, and its magnitude,

$$E=|\mathbf{E}|=\frac{1}{R}\left|\frac{d\varphi}{d\theta}(\theta)\right|, \tag{22}$$

is of the order $1/R$. The field $\mathbf{E}=-\nabla\varphi$ is perpendicular to the radius vector. Thus, the charge near the origin does not create a radial force at all, and one can expect that replacing the singular vertex by a more realistic gap between the electrodes would change the remote fields only slightly (see more detailed explanation in Sec. VIII). We note also that despite the nonmonotonicity of the charge density in our model, $\mathbf{E}$ is always aligned with the direction of increasing θ.

Finite electrodes with gap

This model assumes that each electrode is represented by a line segment between the points $r=k$ and $r=L$, i.e., the closest and the furthest point of each electrode to the origin are k and L, respectively. We cannot study analytically a high-charge-density situation in the case of finite electrodes, and our next step will involve a brief consideration of a much simpler problem when the charge density is negligible. When the gap is absent, $k=0$, the electrostatic field between the infinite electrodes[6] has the form

$$\varphi_0=V\frac{\theta}{\Theta};\quad 0\leq\theta\leq\Theta. \tag{23}$$

For finite electrodes with gap, this potential is distorted for small r and at distances comparable with the electrode length. We study in the Appendix the case $\Theta=\pi$ (which can be easily generalized to any $0<\Theta<2\pi$) with no space charge, when $k\ll L$. The potential equation, Eq. (23), corresponding to $k=0$, $L=\infty$ is modified only slightly when $k\ll r\ll L$:

$$\phi(r,\theta)\approx\frac{V}{\pi}\left[\theta+\left(\frac{r^2}{4L^2}+\frac{k^2}{4r^2}\right)\sin 2\theta\right]. \tag{24}$$

The calculation of corrections for the case with the space charge is much more difficult, but we believe that they are of the same order as in Eq. (24), because the charges between the electrodes will tend to mask the influence of their remote parts. Therefore a charge whose distance $r(\theta)$ from the origin is within some intermediate region, say

$$5k<r(\theta)<0.25L, \tag{25}$$

moves along an almost unperturbed trajectory. Inequalities [Eq. (25)], together with Table I, then allow to apply our results approximately to a part of system in more realistic conditions. While without the gap, $k=0$, the current density [Eq. (13)] $J(r)$ is not integrable, in reality the integral of $J(r)$ in r would be finite and of the order of $1/k$, but very difficult to evaluate. Being cautious one can eliminate the trajectories which do not satisfy Eq. (25) and thus reliably compute the total current collected by a finite part of the anode.

VI. APPLICATIONS

Our analytic study of the space-charge-limited flow in a greatly idealized geometry leading to curved particle trajectories may be useful as a test case for some numerical methods used to study much more complicated geometries. It may also be tested by experiment.

A. Numerical methods

To be specific, let us consider the region in Fig. 4 (with the interelectrode angle Θ) whose boundaries are (i) a cath-

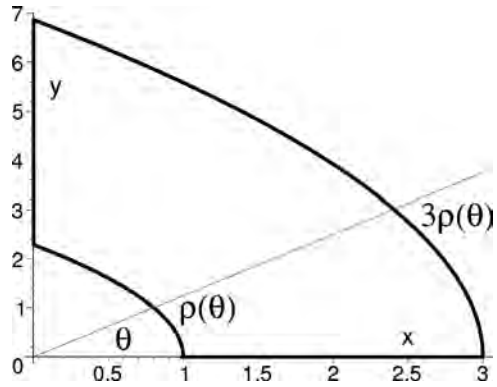

FIG. 5. Closed box with space-charge-limited flow when $\Theta=\pi/2$, $\rho=\sqrt{x^2+y^2}$.

ode interval $[a,b]$, (ii) the anode interval $[\rho(\Theta)a,\rho(\Theta)b]$, (iii) the curve $a\rho(\theta)$ representing the trajectory of a charge moving from a to $\rho(\Theta)a$, and (iv) the trajectory $b\rho(\theta)$ from b toward $b\rho(\Theta)$. In this region all the charged particles emitted by the cathode segment $[a,b]$ are confined to the chosen area and do not cross its boundaries. Numerical calculations of the current and potential for such a region, whose boundary potentials are obtained from the solution in Sec. III, should agree with the results for the infinite wedge. An illustrative example of such a region, delineated by the solid lines, with $\Theta=\pi/2$, $a=1$, $b=3$, is given in Fig. 5. The function $\rho(\theta)$ in Table II defines the shape of the curved sides, i.e., $a\rho(\theta)$ and $b\rho(\theta)$, at 11 points.

The potentials of the straight segments $[a,b]$ and $[a\rho(\Theta),b\rho(\Theta)]$ $(\rho(\pi/2)=2.289)$ are 0 and V, respectively, while the potentials of curved sides $V\psi(\theta)$ are given by $\psi(\theta)$ at the same 11 points in Table II as a function of the angle θ.

More detailed information on ψ and ρ can be easily obtained by solving Eqs. (10) and (11) and using Eqs. (14) and (21). The result of a numerical computation of the current in the anode interval $[2.289a<r<2.289b]$ should be described by Eq. (13), where $h(\pi/2)=0.365$.

B. Experimental testing

The systems considered so far are effectively two-dimensional, i.e., they are infinite in the third dimension perpendicular to the plane in Fig. 4. An experimental check on the model using finite electrodes and a gap between them can be done by assuming that in the third, i.e., z, direction the electrodes have a finite width $2W$: $-W\le z\le W$. Take electrodes of length L, gap $k\ll L$, with an angle Θ between them. Choose a rectangle in the anode by inserting very narrow insulators (dielectric films) in such a way that this isolated patch of the anode collects only almost unperturbed charge trajectories (see Appendix and Sec. IV) while keeping the same potential at all points of the anode. In the case $\Theta=\pi/2$, the sides of this rectangle parallel to the wedge axis should be located between $y_{\min}=d_1\ge 2.5\cdot 2.3k\approx 6k$ and $y_{\max}=d_2\le 0.4L$, while the sides parallel to the plane in Fig. 4 are between $z_{\min}=-W+0.6L$ and $z_{\max}=W-0.6L$, i.e., $W>0.6L$. Thus, we get an area of the anode where the current density is described to a good approximation by Eqs. (13) and (14). By integrating Eq. (13) we evaluate the current into the rectangle above,

$$I=\frac{V^{3/2}Q}{4\pi}\sqrt{\frac{2e}{m}}h(\Theta),\quad Q=2(W-0.6L)\left(\frac{1}{d_1}-\frac{1}{d_2}\right). \tag{26}$$

The insulated anodic area can be of an arbitrary shape, but sitting inside the chosen rectangle, then only the parameter Q in Eq. (26) is to be modified. The corrections in Eq. (26) can be estimated using Eq. (24) and the results of this section. The cathode for this quasi-infinite system should have the same dimensions as the whole anode, i.e., $L\times 2W$, with the same gap k.

For reference we note that the computed $h(\Theta)$ is equal to 0.849, 0.365, 0.436, and 0.660 for $\Theta=\pi/4$, $\pi/2$, $3\pi/4$, and π, respectively (see Fig. 3). An interesting feature to consider is the dependence of the current [Eq. (13)] on the angle θ. After reaching a minimum the current grows and then becomes almost constant. This effect is due to the higher current density near the electrode junction and a significant component of the electron velocity parallel to the anode. Thus, the charges, emitted close to the origin, become a more important component of the total current when Θ increases. Near the cathode the current density at a fixed r decreases, as expected, when we increase the interelectrode distance (and Θ).

VII. LOW-DENSITY CURRENT

Here we compute the trajectories of individual particles in the case when the charge density is negligible. The field is given by Eq. (23), and the charge dynamics is governed by Eqs. (17) and (18). As $\partial\varphi/\partial\theta=$const, the first equation in Eq. (17) yields after one integration,

$$r^2\dot{\theta}=\frac{eV}{m\Theta}t. \tag{27}$$

Combining Eqs. (17) and (27) and using Eq. (18) yields in dimensionless variables

$$\rho^3\frac{d^2\rho}{d\tau^2}=\tau^2,\quad \theta(\tau)=\frac{1}{2}\left[\left(\frac{d\rho}{d\tau}\right)^2+\frac{\tau^2}{\rho^2}\right],$$
$$\text{where}\ \ \rho(0)=1,\quad \frac{d\rho}{d\tau}(0)=0. \tag{28}$$

The differential Eqs. (28), define, as does Eq. (19), in a para-

TABLE II. Data for simulations.

θ	0	0.05π	0.1π	0.15π	0.2π	0.25π	0.3π	0.35π	0.4π	0.45π	0.5π
ρ	1	1.0074	1.0302	1.0696	1.1282	1.2097	1.3199	1.4673	1.6642	1.9290	2.2890
ψ	0	0.04284	0.10817	0.18670	0.27482	0.37243	0.47880	0.59401	0.71856	0.85340	1.0

TABLE III. Distance of a particle from the origin versus the angle θ when the space charge is negligible.

θ	0	0.1π	0.3π	0.5π	0.6π	0.7π	0.8π	0.9π	π	1.2π	1.5π	1.8π	1.9π	2π
ρ	1	1.008	1.077	1.24	1.37	1.55	1.80	2.15	2.67	4.69	17.5	133	305	743

metric form (τ is the parameter) a universal shape $\rho(\theta)$ for the trajectories of all charged particles. The result of a numerical solution of Eq. (28) is shown by the solid curve in Fig. 1. In addition, we developed Table III to cover larger values of θ up to $\Theta=2\pi$, where the particle goes very far from the starting position $\rho(0)=1$.

The particle moves initially almost along the electric field line (Fig. 1) when $\theta<\pi/3$. This is different from the case with strong cathode emission, where at $\theta=\pi/3$ the charge is already 40% further from the origin. For larger θ it deviates more since the field is weaker further out, and it would hit the anode at $\sim 10^3$ (in units of its emission point) after the complete circle (see Table III), but this would still be more than 10 times closer to the origin than in the case of unlimited emission in Table I.

A calculation of the low-density current, for a given cathode emission, is completely straightforward using the normal (to the anode) component of the flow, $J=\dot{\theta}r$, at Θ.

1. When the current density at the cathode $j_c(x)$ is fixed (and small!), we have, due to the universality of particle trajectories, the current density at a point r of the anode

$$j_a(r)=\frac{1}{\rho(\Theta)}j_c[r/\rho(\Theta)]. \tag{29}$$

A simple estimate shows that for validity of this approach to the low-density flow, the cathode current $j_c(x)$ must satisfy the inequality

$$j_c(x)\ll\frac{d^2}{x^2}j_0, \tag{30}$$

where j_0 is the Child–Langmuir current Eq. (15) with the same V. Note that if Eq. (29) holds, j_a is independent of V; it gives only the normal to the anode component of the current density vector whose absolute value is larger. In this case an increase of particle velocities, by gaining energy from the field, is compensated by a decrease of their density and thus the current is conserved.

2. When the cathode current $j_c(x)$ is not fixed but proportional to the electric field $E(x)$ at $\theta=0$ (modeling in such a way the field emission), i.e.,

$$j_c(x)=\lambda E(x)=\frac{\lambda V}{\Theta x}, \tag{31}$$

where we used Eq. (24). The upper bound on the emission parameter λ for using the low-density approximation is to be determined with the help of Eq. (30). By combining Eqs. (31), (30), (15), and (25) we obtain

$$\lambda\ll 0.02\frac{\Theta}{\pi k}\sqrt{\frac{2eV}{m}}. \tag{32}$$

When this inequality holds and $r(\theta)=r/\rho(\theta)$ satisfies Eq. (25), the anode current has the form

$$j_a(r)=\frac{V\lambda}{\Theta r}.$$

VIII. DISCUSSION

Here we offer a qualitative physical explanation of why our model with infinite charge near the origin can be used in more realistic conditions and why the nonmonotonic charge distribution in Fig. 4 is the stationary state of flow. The key point is to study how the charges near the vertex affect the overall charge density and how their singular behavior manifests itself far away.

It is easy to see that the infinite charge near $r=0$ does not push more remote charges with an infinite force, and even according to the solution Eq. (12) the total force has no radial component. For illustration we consider again the case $\Theta=\pi$. A single charge e, located at a distance d from a conducting surface, say at the point $(d,\pi/2)$, creates an electric field $\mathbf{E}$ at a point $(R\gg d,\alpha)$ with dominant dipole components,

$$E_r=\frac{4ed\sin\alpha}{R^3},\quad E_\alpha=-\frac{2ed\cos\alpha}{R^3}, \tag{33}$$

where E_r is directed along the radius vector and E_α is perpendicular to it. Using Eqs. (7) and (22) the components of electrostatic force exerted upon a single charge at (R,α) by the space charge located near the origin $r\le k$ can be found as integrals

$$\mathbf{F}=\int_0^k rdr\int_0^\Theta \mathbf{E}n(r,\theta)d\theta.$$

They are of the order k/R^3 and $F_r\propto\sin\alpha$, $F_\alpha\propto-\cos\alpha$; therefore, the contribution of a small sector with $r<k$ to the total force acting on remote charges (which is proportional to $1/R$) is negligible for large R. The spatial structure of the charge distribution makes the radial part of this force disappear completely.

These results show the applicability of our model to the case with a finite gap k, because the presence or absence of an infinite charge near the wedge origin modifies the field only to terms of order R^{-3} [see Eq. (33)]. These terms are negligible compared with Eq. (22). Equation (33) also explains the minimum of the charge density for intermediate values of θ. When $\Theta>\pi/2$, the charged particles are pushed to both electrodes by F_θ and this determines the spatial charge structure and the potential field of the stationary distribution. For a system with $\Theta<\pi$, the repulsive force from charges located near the origin is "screened" by the electrodes even more effectively.

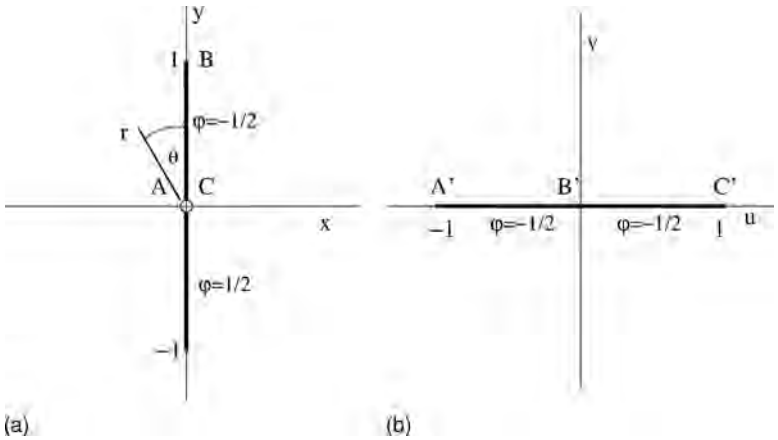

FIG. 6. (a) Complex $z=x+iy$ plane. (b) Complex $w=u+iv$ plane.

IX. CONCLUSION

We computed the distributions of current, electric potential, and the particle trajectories in two extreme situations with very low and very high emissivities of the cathode. The "infinite" emissivity in fact does not necessarily create a large charge density. This is determined by the applied voltage and especially the angle Θ of the wedge. We expect that when the electrodes are of a finite length L and have gap $k>0$, the potential φ gets corrections of second order in r/L and k/r, as in Eq. (24), even for an infinite emissivity case. Therefore the flow at distances r from the origin will be disturbed only a little if Eq. (25) holds.

ACKNOWLEDGMENTS

Comments by R. Barker and K. Jensen are greatly appreciated. This research was supported by the U.S. Air Force Office of Scientific Research, Grant No. F49620-01-0154.

APPENDIX: MATHEMATICAL JUSTIFICATION OF GENERALIZATION

The potential Eq. (23) is a solution of the Laplace equation for the case of infinite electrodes which make the angle Θ in Fig. 1. We will show here, using the example of $\Theta=\pi$, that the results above can be applied with some restrictions when the electrodes are finite and separated by a finite interval.

1. Let us find the potential created by two electrodes vertically placed along the y-axis of the unit length [see Fig. 6(a)], whose potentials are $-1/2$ and $+1/2$.

Due to the symmetry the field in the upper half plane is the same as the solution φ of the Dirichlet problem (plus 1/2), when the x-axis has the zero potential while the line segment $x=0$, $0<y\leq 1$ has the potential 1/2. Treating the plane in Fig. 6(a) as the complex one, we map its upper half conformally onto the upper half plane w in Fig. 6(b) using[7] the function

$$w=u+iv=\sqrt{z^2+1}, \quad z=x+iy, \tag{A1}$$

where the points A, B, C in Fig. 6(a) correspond to A′, B′, C′, respectively, in Fig. 6(b). Thus, the u-axis has the potential zero, except the interval $-1\leq u\leq 1$, whose potential is $-1/2$. The solution for the potential in the whole half plane $v>0$ is

$$\varphi=\frac{1}{2}-\frac{v}{\pi}\int_{-1}^{1}\frac{\varphi(\eta,0)d\eta}{(\eta-u)^2+v^2}=\frac{1}{4}-\frac{1}{2\pi}\arctan\frac{1-u^2-v^2}{2v}. \tag{A2}$$

The addition of 1/2 in Eq. (A2) makes φ in the polar coordinates exactly corresponding to the potential in Fig. 1, where the half axis $x>0$ has the zero potential (but not $-1/2$).

The area near the origin in the second quadrant in Fig. 6(a) corresponds to $u\approx -1$, $0<v<1$ in Fig. 6(b). Expressing u and v in the polar coordinates $x=-r\sin\theta$, $y=r\cos\theta$ with the help of Eq. (A1) we have

$$u\approx -1+\frac{r^2}{2}\cos 2\theta+\frac{r^4}{8}\cos 4\theta+\frac{r^6}{16}\cos 6\theta,$$

$$v\approx \frac{r^2}{2}\sin 2\theta+\frac{r^4}{8}\sin 4\theta+\frac{r^6}{16}\sin 6\theta. \tag{A3}$$

By substituting Eq. (A3) in Eq. (A2), we compute φ in the same variables as in Eq. (5),

$$\varphi(r,\theta)=\frac{\theta}{\pi}+\frac{r^2\sin 2\theta}{4\pi}[1+r^2(\cos^2\theta-1/4)]+O(r^6). \tag{A4}$$

The relative difference between Eq. (A4) and Eq. (23), where one should take $V=1$, $\Theta=\pi$ reaches its maximum at about $r^2/2$ near $\theta=0$ and $\theta=\pi$.

2. We consider now two infinite electrodes in the same horizontal plane separated by an interval $D=2k$ (see the cross section in Fig. 7).

The left one is the anode, and the right electrode is the cathode whose potential is zero. The electric field structure of this system, which is shown in Fig. 7, is obtained by using a simple conformal map[7] $z=k\cosh w$. The lines $u=const$, $v=const$ from the plane $w=u+iv$ are converted into the sets of ellipses

$$1=\frac{x^2}{k^2\cosh^2 u}+\frac{y^2}{k^2\sinh^2 u}, \tag{A5}$$

and hyperbolas

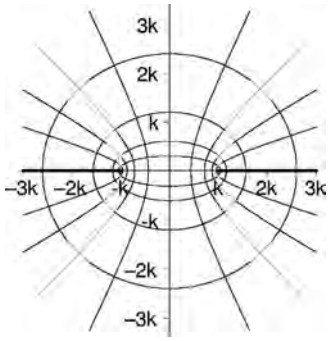

FIG. 7. Infinite electrodes with a gap $D=2k$ between them.

$$1 = \frac{x^2}{k^2 \cos^2 v} - \frac{y^2}{k^2 \sin^2 v}, \tag{A6}$$

respectively, in the complex z plane, where points $x=\pm k$, $y=0$ are their foci.

Equations (A5) and (A6) are the solutions of this electrostatic problem: the ellipses represent the electric field lines while the hyperbolas give the equipotentials. Note that if the anode cross section is one of hyperbolas [Eq. (A6)] of Fig. 7 (the y-axis in particular), the vacuum field structure is the same, but $\theta_{max} < \pi$. In the polar coordinates $r=\sqrt{x^2+y^2}$, $\theta = \arctan y/x$ Eq. (A6) gets the form

$$\tan^2 \theta = \tan^2 v - \frac{k^2 \sin^2 v}{r^2 \cos^2 \theta}.$$

Assuming $k^2/r^2 \ll 1$, we solve this equation for the potential of the chosen hyperbola

$$v = \theta + \frac{k^2}{4r^2} \sin 2\theta + O(k^4/r^4). \tag{A7}$$

If the anode potential is V, this solution should be multiplied by the factor V/π.

In the case of unlimited emission the potential is different from Eqs. (A4) and (23), but one might expect that due to $l < \infty$ corrections to the field in Eq. (12) are of the order $r^2/2$, too, because (i) apart from the origin the space-charge density $n(r,\theta)$ rapidly decreases (as r^{-2}), and (ii) the space charge is "masking" the remote form of the electrodes. Though the corrections [Eq. (A7)] can be easily implemented (or discarded), the full disturbance caused by the interelectrode gap is not that straightforward and is discussed in Sec. V.

[1] P. T. Kirsten, G. S. Kino, and W. E. Waters, *Space Charge Flow* (McGraw-Hill, New York, 1967); A. S. Gilmour, Jr., *Microwave Tubes* (Artech House, Dedham, MA, 1986); J. U. R. Pierce, *Theory and Design of Electron Beams* (Van Nostrand, New York, 1954); M. Reiser, *Theory and Design of Charged Particle Beams* (Wiley, New York, 1994).
[2] J. W. Luginsland, Y. Y. Lau, R. J. Umstattd, and J. J. Watrous, Phys. Plasmas **9**, 2371 (2002); F. Hegeler, M. Friedman, M. C. Myers, J. D. Sethian, and S. B. Swanekamp, *ibid.* **9**, 4309 (2002); A. Rokhlenko and J. L. Lebowitz, Phys. Rev. Lett. **91**, 085002 (2003); A. Rokhlenko and J. L. Lebowitz, Phys. Plasmas **11**, 4559 (2004); A. Rokhlenko, J. Appl. Phys. **100**, 013305 (2006).
[3] R. J. Umstattd and J. W. Luginsland, Phys. Rev. Lett. **87**, 145002 (2001); J. W. Luginsland, Y. Y. Lau, and R. M. Gilgenbach, *ibid.* **77**, 4668 (1996); Y. Y. Lau, *ibid.* **87**, 278301 (2001); Y. Y. Lau, P. J. Christenson, and D. Chernin, Phys. Fluids B **5**, 4486 (1993).
[4] V. E. Gollant, A. P. Zhilinsky, and I. E. Sakharov, *Fundamental of Plasma Physics* (Wiley, New York, 1980); F. F. Chen, *Introduction to Plasma Physics and Controlled Fusion* (Plenum Press, New York, 1983).
[5] C. D. Child, Phys. Rev. **32**, 492 (1911); I. Langmuir, *ibid.* **2**, 450 (1913).
[6] J. D. Jackson, *Classical Electrodynamics* (Wiley, New York, 1975).
[7] K. Von Simonyi, *Theoretische Elektrotechnik* (Veb Deutscher Verlag, Berlin, 1956); P. M. Morse and H. Feshbach, *Methods of Theoretical Physics*, (McGraw-Hill, New York, 1953), Vol. 2.